International Journal of Thermal Sciences 49 (2010) 23–35

Contents lists available at ScienceDirect

International Journal of Thermal Sciences

journal homepage: www.elsevier.com/locate/ijts

Thermal analysis of rough micro-fins of variable cross-section by the power series method

Luis I. Díez [a,*], Sergio Espatolero [a], Cristóbal Cortés [a], Antonio Campo [b]

[a] Center of Research of Energy Resources and Consumptions, Department of Mechanical Engineering, University of Zaragoza, María de Luna, 3, 50018 Zaragoza, Spain
[b] Department of Mechanical Engineering, The University of Texas at San Antonio, One UTSA Circle, San Antonio, TX 78249, USA

ARTICLE INFO

Article history:
Received 17 December 2008
Received in revised form
26 May 2009
Accepted 27 May 2009
Available online 24 June 2009

Keywords:
Micro-pin fins
Variable diameter
Rough surfaces
Fin efficiency
Power series

ABSTRACT

Thermal performance of micro-pin fins of variable diameter and rough surface is calculated by means of an approximate procedure based on truncated power series. The geometric effect of roughness is modeled after Bahrami et al. [9], which greatly increases the intricacy of the fin equation, preventing its analytical solution even by symbolic computer codes. The approximate series solution is developed firstly by estimating an adequate number of terms based on convergence to the (known) exact solution of smooth pin fins of the same geometry. Then, residual convergence for an increasing number of terms is studied for the rough fin. Three selected geometries are analyzed, of hyperbolic, trapezoidal and concave parabolic profiles. Influence of surface roughness is evaluated for a wide range of heat transfer conditions; results are discussed in terms of the two primary quantities of interest in fin design, viz., efficiency and effectiveness. Due to the easiness of the present methodology, it can be safely applied to other geometric arrangements involving straight and annular fins.

1. Introduction

A widely used method to enhance heat transfer from walls and tubes to surrounding fluid streams consists in the attachment of pin fin arrays to the surface [1,2]. In this framework, numerous applications can be cited: air-cooled engines, gas–gas or gas–liquid compact heat exchangers, condensers, evaporators, etc. More specifically, applications of micro-fins are continuously rising with ever-increasing requirements for heat transfer dissipation along with severe space and weight limitations. This is the case of microelectronic heat sinks [3], gas turbine blades [4] or thermal actuators [5].

Surfaces manufactured by MEMS technologies usually have some level of roughness [6], strongly dependent on the fabrication process or the materials used. The role of roughness in heat transfer increases as the size of the equipment decreases. Separate experimental works [7,8] have pointed out the heat transfer augmentation introduced by roughness in square and cylindrical pin fins of constant thickness. The geometric effect of roughness has been modeled by Bahrami et al. [9] for the cylindrical, constant-diameter geometry. Analyzing the variation in average cross-sectional and lateral areas, a modified 1-D temperature equation was developed, whose solution showed an increase in heat transfer rate. To the present authors' knowledge, this work is the only one dealing with the problem.

The objective of this paper is to move forward the mathematical analysis into the study of rough micro-pin fins of variable diameter. Chyu et al. [10] refer to different pin fin shapes as an alternative for cooling; the critical geometric parameters that influence heat transfer from a fin array are diameter, length, inter-fin spacing and fin profile. Concerning the latter, there is a subset of tapered profiles capable of transferring larger amounts of heat per unit cross-sectional area at the base than the constant-thickness fin. Among these they are the hyperbolic, convex parabolic and concave parabolic profiles [11].

We arbitrarily select for this study three realistic, truncated pin fin geometries of trapezoidal, hyperbolic and concave parabolic profiles. We deduce the differential equations governing their 1-D temperature distribution by introducing a random isotropic surface roughness and following the method of Ref. [9]. We rule out to manage the exact analytical solution of these equations, since they are highly intricate and likely error-prone. Alternatively, we suggest the implementation of the approximate power series method as a simple way to obtain accurate predictions of the performance of the pin fins. Results are presented for the convergence of the power series and the effect that the roughness

* Corresponding author. Tel.: +34 976 762564; fax: +34 976 732078.
E-mail address: luisig@unizar.es (L.I. Díez).

1290-0729/$ – see front matter © 2009 Elsevier Masson SAS. All rights reserved.
doi:10.1016/j.ijthermalsci.2009.05.013

Nomenclature

A_b	cross-sectional area at the fin base, m^2
A_c	cross-sectional area of the fin, m^2
$\overline{A}_c$	average cross-sectional area of the rough fin, m^2
A_s	surface area of the fin exposed to convection, m^2
$\overline{A}_s$	average surface area of the rough fin exposed to convection, m^2
Bi	Biot number, given by $2r_b h/k$
E	fin effectiveness
e	convergence error
f	fractional error, as defined by Eq. (52)
h	uniform convection coefficient, $W\,m^{-2}\,K^{-1}$
I_ν	modified Bessel function of first kind and order $\nu = 0, 1, 2$
K_ν	modified Bessel function of second kind and order $\nu = 0, 1, 2$
k	fin thermal conductivity, $W\,m^{-1}\,K^{-1}$
L	fin length, m
m	thermo-geometric parameter, m^{-1}
m_σ	mean absolute surface slope
M^2	extended Biot number, as defined by Eq. (20)
n	number of terms retained in the shortened power series
P	fin perimeter, m
q	heat transfer rate, W
q_{ideal}	ideal heat transfer rate, W
r	fin radius, m
$\overline{r}$	average radius of a rough fin, m
r_δ	random variation of the fin radius in the angular direction, m
r_b	radius at the fin base, m
r_L	random variation of the fin radius in the longitudinal direction, m
r_t	radius at the fin tip, m
T	temperature, K
T_b	base temperature, K
T_∞	fluid temperature, K
x	longitudinal coordinate, m
x_b	location of the base for the hyperbolic fin, m
x_t	location of the tip for the hyperbolic fin, m
z	longitudinal coordinate, m
z_b	location of the base for the trapezoidal and concave parabolic fins, m
z_t	location of the tip for the trapezoidal and concave parabolic fins, m

Greek symbols

ε	relative roughness, as defined by Eq. (27)
ϕ	dimensionless coordinate, as defined by Eq. (16a)
η	fin efficiency
λ	length of the arc of the fin profile, m
θ	dimensionless temperature, as defined by Eq. (14a)
σ	isotropic surface roughness, m
σ_δ	fin surface roughness in the angular direction, m
σ_L	fin surface roughness in the longitudinal direction, m
ω	geometric ratio, as defined by Eq. (16b)
ξ	geometric ratio, as defined by Eq. (14c)
ψ	dimensionless coordinate, as defined by Eq. (14b)

Subindexes

h	hyperbolic
p	concave parabolic
t	trapezoidal

bears on the fin efficiency and effectiveness, under different heat transfer conditions and geometric parameters of the pin fin. Analysis is pursued in dimensionless form, in order to cover a wide range of cases.

2. Formulation for pin fins of variable profile and smooth surface

For a constant thermal conductivity k and a uniform convection coefficient h, the steady-state temperature descent along a thin, truncated pin fin of a variable radius $r(x)$, like those illustrated in Fig. 1, obeys the quasi 1-D fin equation

$$\frac{d^2T}{dx^2} + \frac{1}{A_c}\frac{dA_c}{dx}\frac{dT}{dx} - \frac{hP}{kA_c}(T - T_\infty) = 0 \tag{1}$$

where A_c and P are cross-sectional area and perimeter, given by

$$A_c(x) = \pi r(x)^2 \tag{2}$$

$$P(x) = 2\pi r(x) \tag{3}$$

In Eq. (1), we adopt the length-of-arc approximation: $(dr/dx)^2 \ll 1$, so that the derivative of lateral area can be substituted by perimeter, $dA_s/dx \approx P$, in the last term. This assumption is very common in fin theory and completely reasonable for normal, slender fins.

Imposed boundary conditions are also those common in fin analysis, namely, prescribed temperature at the fin base and negligible heat loss at the fin tip:

$$T|_{x=x_b} = T_b \tag{4a}$$

$$\frac{dT}{dx}\Big|_{x=x_t} = 0 \tag{4b}$$

Fig. 1 sketches the three geometries of truncated pin fins selected to carry out the present study: hyperbolic, trapezoidal and concave parabolic pin fins. The hyperbolic pin fin is created with a smooth profile of variable radius:

$$r_h(x) = r_b\frac{x_b}{x} \tag{5}$$

Substituting this radius into Eqs. (1)–(3), we get the differential equation for the temperature descent along x (in $x_b \le x \le x_t$):

$$\frac{d^2T_h}{dx^2} - \frac{2}{x}\frac{dT_h}{dx} - 2\frac{x}{x_b}m^2(T_h - T_\infty) = 0 \tag{6}$$

where m is the thermo-geometric parameter, given by

$$m^2 = \frac{h}{kr_b} \tag{7}$$

To obtain the differential equation for the trapezoidal and concave parabolic pin fins, we firstly introduce for convenience the longitudinal coordinate z (see also Fig. 1):

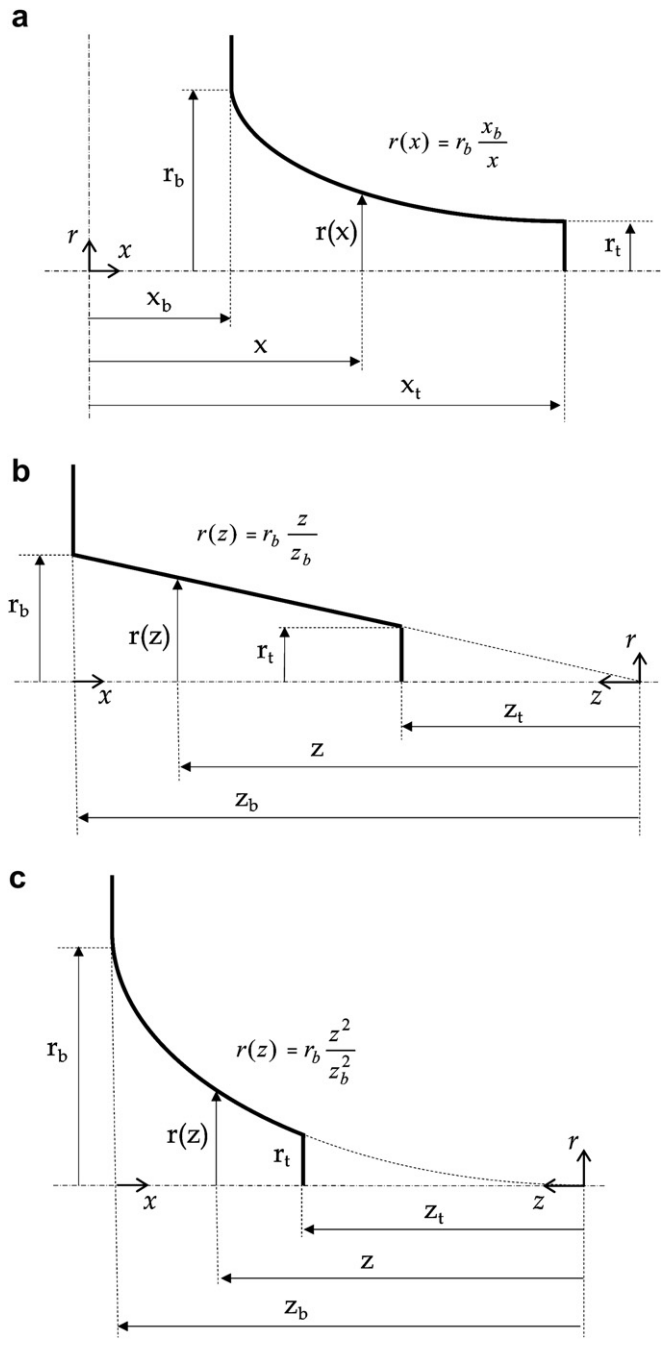

Fig. 1. Sketches of the truncated pin fins of variable profile: a) hyperbolic, b) trapezoidal, c) concave parabolic.

$$z = z_b - x \tag{8}$$

which transforms Eq. (1) to

$$\frac{d^2T}{dz^2} + \frac{1}{A_c}\frac{dA_c}{dz}\frac{dT}{dz} - \frac{hP}{kA_c}(T - T_\infty) = 0 \tag{9}$$

where it is understood that $A_c(z)$ and $P(z)$ are calculated as in Eqs. (2) and (3) with z replacing x. Trapezoidal and concave parabolic pin fins are then created with smooth profiles of variable radius given, respectively, by

$$r_t(z) = r_b\frac{z}{z_b} \tag{10}$$

$$r_p(z) = r_b\left(\frac{z}{z_b}\right)^2 \tag{11}$$

The corresponding differential equations are (in $z_t \le z \le z_b$):

$$\frac{d^2T_t}{dz^2} + \frac{2}{z}\frac{dT_t}{dz} - 2\frac{z_b}{z}m^2(T_t - T_\infty) = 0 \tag{12}$$

$$\frac{d^2T_p}{dz^2} + \frac{4}{z}\frac{dT_p}{dz} - 2\frac{z_b^2}{z^2}m^2(T_p - T_\infty) = 0 \tag{13}$$

where the thermo-geometric parameter m is defined by Eq. (7).

Upon defining dimensionless temperature θ, dimensionless coordinate ψ and geometric ratio ξ in this way:

$$\theta = \frac{T - T_\infty}{T_b - T_\infty} \tag{14a}$$

$$\psi = \frac{x}{x_t} \tag{14b}$$

$$\xi = \frac{x_b}{x_t} \tag{14c}$$

the equation of the hyperbolic pin fin, Eq. (6), transforms (in $\xi \le \psi \le 1$) to

$$\frac{d^2\theta_h}{d\psi^2} - \frac{2}{\psi}\frac{d\theta_h}{d\psi} - 2\frac{x_t^3}{x_b}\psi m^2\theta_h = 0 \tag{15a}$$

Analogously, dimensionless forms of Eqs. (12) and (13) become (in $\omega \le \phi \le 1$):

$$\frac{d^2\theta_t}{d\phi^2} + \frac{2}{\phi}\frac{d\theta_t}{d\phi} - 2\frac{z_b^2}{\phi}m^2\theta_t = 0 \tag{15b}$$

$$\frac{d^2\theta_p}{d\phi^2} + \frac{4}{\phi}\frac{d\theta_p}{d\phi} - 2\frac{z_b^2}{\phi^2}m^2\theta_p = 0 \tag{15c}$$

where θ is the same, Eq. (14a), and the other dimensionless variables are given by

$$\phi = \frac{z}{z_b} \tag{16a}$$

$$\omega = \frac{z_t}{z_b} \tag{16b}$$

In dimensionless terms, boundary conditions for the hyperbolic pin fin are:

$$\theta_h|_{\psi=\xi} = 1 \tag{17a}$$

$$\frac{d\theta_h}{d\psi}\Big|_{\psi=1} = 0 \tag{17b}$$

whereas for the trapezoidal and concave parabolic pin fins we get

$$\theta_t|_{\phi=1} = 1, \quad \theta_p|_{\phi=1} = 1 \tag{18a}$$

$$\frac{d\theta_t}{d\phi}\Big|_{\phi=\omega} = 0, \quad \frac{d\theta_p}{d\phi}\Big|_{\phi=\omega} = 0 \tag{18b}$$

A convenient alternate form of Eq. (15) is

$$\psi\frac{d^2\theta_h}{d\psi^2}-2\frac{d\theta_h}{d\psi}-2M_h^2\psi^2\theta_h=0 \tag{19a}$$

$$\phi\frac{d^2\theta_t}{d\phi^2}+2\frac{d\theta_t}{d\phi}-2M_t^2\theta_t=0 \tag{19b}$$

$$\phi\frac{d^2\theta_p}{d\phi^2}+4\frac{d\theta_p}{d\phi}-\frac{2}{\phi}M_p^2\theta_p=0 \tag{19c}$$

where M^2 is an extended Biot number defined as

$$M_h^2=\frac{x_t^3}{x_b}m^2=\frac{x_t^3}{x_b}\frac{h}{kr_b} \tag{20a}$$

$$M_t^2=M_p^2=z_b^2m^2=z_b^2\frac{h}{kr_b} \tag{20b}$$

The exact solution of Eq. (19) subjected to the boundary conditions in Eq. (17) or (18) has been determined with the symbolic code Mathematica 5.2 [12]. After the algebra is done, dimensionless temperature distributions are obtained for

1) the hyperbolic pin fin,

$$\begin{aligned}\theta_h(\psi)=&\frac{1}{\xi^{3/2}}\cdot\left[\sqrt{2}M_h\psi^{3/2}I_1\left(\frac{2\sqrt{2}}{3}M_h\psi^{3/2}\right)K_0\left(\frac{2\sqrt{2}}{3}M_h\right)\right.\\&-3\psi^{3/2}I_1\left(\frac{2\sqrt{2}}{3}M_h\psi^{3/2}\right)K_1\left(\frac{2\sqrt{2}}{3}M_h\right)\\&+\sqrt{2}M_h\psi^{3/2}K_1\left(\frac{2\sqrt{2}}{3}M_h\psi^{3/2}\right)I_0\left(\frac{2\sqrt{2}}{3}M_h\right)\\&+3\psi^{3/2}K_1\left(\frac{2\sqrt{2}}{3}M_h\psi^{3/2}\right)I_1\left(\frac{2\sqrt{2}}{3}M_h\right)\\&+\sqrt{2}M_h\psi^{3/2}K_1\left(\frac{2\sqrt{2}}{3}M_h\psi^{3/2}\right)I_2\left(\frac{2\sqrt{2}}{3}M_h\right)\\&\left.+\sqrt{2}M_h\psi^{3/2}I_1\left(\frac{2\sqrt{2}}{3}M_h\psi^{3/2}\right)K_2\left(\frac{2\sqrt{2}}{3}M_h\right)\right]\cdot\\&\left[\sqrt{2}M_hI_1\left(\frac{2\sqrt{2}}{3}M_h\xi^{3/2}\right)K_0\left(\frac{2\sqrt{2}}{3}M_h\right)\right.\\&-3I_1\left(\frac{2\sqrt{2}}{3}M_h\xi^{3/2}\right)K_1\left(\frac{2\sqrt{2}}{3}M_h\right)\\&+\sqrt{2}M_hK_1\left(\frac{2\sqrt{2}}{3}M_h\xi^{3/2}\right)I_0\left(\frac{2\sqrt{2}}{3}M_h\right)\\&+3K_1\left(\frac{2\sqrt{2}}{3}M_h\xi^{3/2}\right)I_1\left(\frac{2\sqrt{2}}{3}M_h\right)\\&+\sqrt{2}M_hK_1\left(\frac{2\sqrt{2}}{3}M_h\xi^{3/2}\right)I_2\left(\frac{2\sqrt{2}}{3}M_h\right)\\&\left.+\sqrt{2}MI_1\left(\frac{2\sqrt{2}}{3}M_h\xi^{3/2}\right)K_2\left(\frac{2\sqrt{2}}{3}M_h\right)\right]^{-1}\end{aligned} \tag{21a}$$

2) the trapezoidal pin fin,

$$\begin{aligned}\theta_t(\phi)=&\frac{1}{\phi^{1/2}}\cdot\left[\sqrt{2}M_t\omega^{1/2}I_1\left(2\sqrt{2}M_t\phi^{1/2}\right)K_0\left(2\sqrt{2}M_t\omega^{1/2}\right)\right.\\&+I_1\left(2\sqrt{2}M_t\phi^{1/2}\right)K_1\left(2\sqrt{2}M_t\omega^{1/2}\right)\\&+\sqrt{2}M_t\omega^{1/2}I_0\left(2\sqrt{2}M_t\omega^{1/2}\right)K_1\left(2\sqrt{2}M_t\phi^{1/2}\right)\\&-I_1\left(2\sqrt{2}M_t\omega^{1/2}\right)K_1\left(2\sqrt{2}M_t\phi^{1/2}\right)\\&+\sqrt{2}M_t\omega^{1/2}I_2\left(2\sqrt{2}M_t\omega^{1/2}\right)K_1\left(2\sqrt{2}M_t\phi^{1/2}\right)\\&\left.+\sqrt{2}M_t\omega^{1/2}I_1\left(2\sqrt{2}M_t\phi^{1/2}\right)K_2\left(2\sqrt{2}M_t\omega^{1/2}\right)\right]\cdot\\&\left[\sqrt{2}M_t\omega^{1/2}I_1\left(2\sqrt{2}M_t\right)K_0\left(2\sqrt{2}M_t\omega^{1/2}\right)\right.\\&+\sqrt{2}M_t\omega^{1/2}I_0\left(2\sqrt{2}M_t\omega^{1/2}\right)K_1\left(2\sqrt{2}M_t\right)\\&-I_1\left(2\sqrt{2}M_t\omega^{1/2}\right)K_1\left(2\sqrt{2}M_t\right)\\&+\sqrt{2}M_t\omega^{1/2}I_2\left(2\sqrt{2}M_t\omega^{1/2}\right)K_1\left(2\sqrt{2}M_t\right)\\&+I_1\left(2\sqrt{2}M_t\right)K_1\left(2\sqrt{2}M_t\omega^{1/2}\right)\\&\left.+\sqrt{2}M_t\omega^{1/2}I_1(2\sqrt{2}M_t)K_2(2\sqrt{2}M_t\omega^{1/2})\right]^{-1}\end{aligned} \tag{21b}$$

3) the concave parabolic pin fin,

$$\begin{aligned}\theta_p(\phi)=&\left[\left(-3+\sqrt{9+8M_p^2}\right)\omega^{\left[-3/2+1/2(\sqrt{9+8M_p^2})\right]}\right.\\&\phi^{\left[-3/2-1/2(\sqrt{9+8M_p^2})\right]}+\left(3+\sqrt{9+8M_p^2}\right)\\&\left.\omega^{\left[-3/2-1/2(\sqrt{9+8M_p^2})\right]}\phi^{\left[-3/2+1/2(\sqrt{9+8M_p^2})\right]}\right]\cdot\\&\left[3\omega^{\left[-3/2-1/2(\sqrt{9+8M_p^2})\right]}-3\omega^{\left[-3/2+1/2(\sqrt{9+8M_p^2})\right]}\right.\\&+\sqrt{9+8M_p^2}\omega^{\left[-3/2-1/2(\sqrt{9+8M_p^2})\right]}\\&\left.+\sqrt{9+8M_p^2}\omega^{\left[-3/2+1/2\left(\sqrt{9+8M_p^2}\right)\right]}\right]^{-1}\end{aligned} \tag{21c}$$

In the preceding equations, I_ν and K_ν stand for the modified Bessel functions of first and second kind and order $\nu=0, 1, 2$ [13].

Usually the heat transfer rate q from fins to a fluid is computed indirectly with the fin efficiency, given by

$$\eta_h=\frac{q_h}{q_{ideal}}=\frac{q_h}{hA_s(T_b-T_\infty)}=-\frac{k}{h}\frac{A_b}{A_s}\frac{1}{x_t}\frac{d\theta_h}{d\psi}\Big|_{\psi=\xi} \tag{22a}$$

$$\eta_t=\frac{q_t}{q_{ideal}}=\frac{q_t}{hA_s(T_b-T_\infty)}=-\frac{k}{h}\frac{A_b}{A_s}\frac{1}{z_b}\frac{d\theta_t}{d\phi}\Big|_{\phi=1} \tag{22b}$$

$$\eta_p=\frac{q_p}{q_{ideal}}=\frac{q_p}{hA_s(T_b-T_\infty)}=-\frac{k}{h}\frac{A_b}{A_s}\frac{1}{z_b}\frac{d\theta_p}{d\phi}\Big|_{\phi=1} \tag{22c}$$

where A_b is the cross-sectional area at the fin base and A_s is the surface area of the fin exposed to convection.

Another variable of comparable interest in the thermal analysis of fins is the so-called fin effectiveness, defined as:

$$E_h = \frac{q_h}{hA_b(T_b - T_\infty)} = -\frac{k}{h}\frac{1}{x_t}\frac{d\theta_h}{d\psi}\Big|_{\psi=\xi} \tag{23a}$$

$$E_t = \frac{q_t}{hA_b(T_b - T_\infty)} = -\frac{k}{h}\frac{1}{z_b}\frac{d\theta_t}{d\phi}\Big|_{\phi=1} \tag{23b}$$

$$E_p = \frac{q_p}{hA_b(T_b - T_\infty)} = -\frac{k}{h}\frac{1}{z_b}\frac{d\theta_p}{d\phi}\Big|_{\phi=1} \tag{23c}$$

It is clear that the numerical evaluation of the dimensionless temperatures θ with Eq. (21), fin efficiency η with Eq. (22) and fin effectiveness E with Eq. (23) –for which the evaluation of the temperature derivative at the base is required–, constitutes a rather laborious and error-prone task. Certainly, these drawbacks are even more pronounced when the surface roughness is incorporated into the analysis, a feature that necessitates very complex differential equations and, consequently, more intricate exact solutions. This difficult topic appears in the following section wherein the power series method will be adopted.

3. Calculation of micro-pin fins with rough surfaces

A micro-pin fin of variable average radius $\bar{r}(x)$ is considered now (see Fig. 2). Following [9] strictly, we assume that the surface roughness is random and obeys a Gaussian probability distribution, both in the angular and longitudinal directions. The picture in Fig. 2 is intentionally not scaled; the surface irregularities actually are shallow variations of the surface height and slope.

Under this circumstance, an exact value of the local radius cannot be used for calculating temperatures in rough fins. Therefore, probabilities for specific radii have to be managed. For this purpose, the radius at every point (x, θ) of the variable-profile pin fin is defined as

$$r(x,\theta) = \bar{r}(x) + r_\delta + r_L \tag{24}$$

where r_δ and r_L stand for random variables used to represent the variation around the mean radius $\bar{r}(x)$ along the angular and the longitudinal directions, respectively. The standard deviation of r_δ is the surface roughness σ_δ in the angular direction and the standard deviation of r_L is the surface roughness σ_L in the longitudinal direction; both quantities follow a Gaussian probability distribution given as

$$\Theta(r_\delta) = \frac{1}{\sqrt{2\pi}\sigma_\delta}\exp\left(-\frac{r_\delta^2}{2\sigma_\delta^2}\right) \tag{25a}$$

$$\Theta(r_L) = \frac{1}{\sqrt{2\pi}\sigma_L}\exp\left(-\frac{r_L^2}{2\sigma_L^2}\right) \tag{25b}$$

Eq. (24) means that the value of local radius is a double superposition of random independent variations around the mean, taking the probability distributions from Eq. (25). In a general case, the standard deviations of r_δ and r_L can be different. Nevertheless, we are going to postulate the simplification pertinent to isotropic roughness, that is, $\sigma = \sigma_\delta = \sigma_L$.

Surface roughness produces geometric modifications of the fin that have an effect in heat transfer. If the roughness profile is random and their peaks and valleys are of a magnitude much smaller than the macroscopic dimensions (i.e., the relative roughness is $\varepsilon = \sigma/r \ll 1$), a statistical model can be conceived. It is based on the fact that, for the conditions given, every particular realization of the rough surface can be represented by its average dimensions, and that this average is equivalent to the statistical mean.

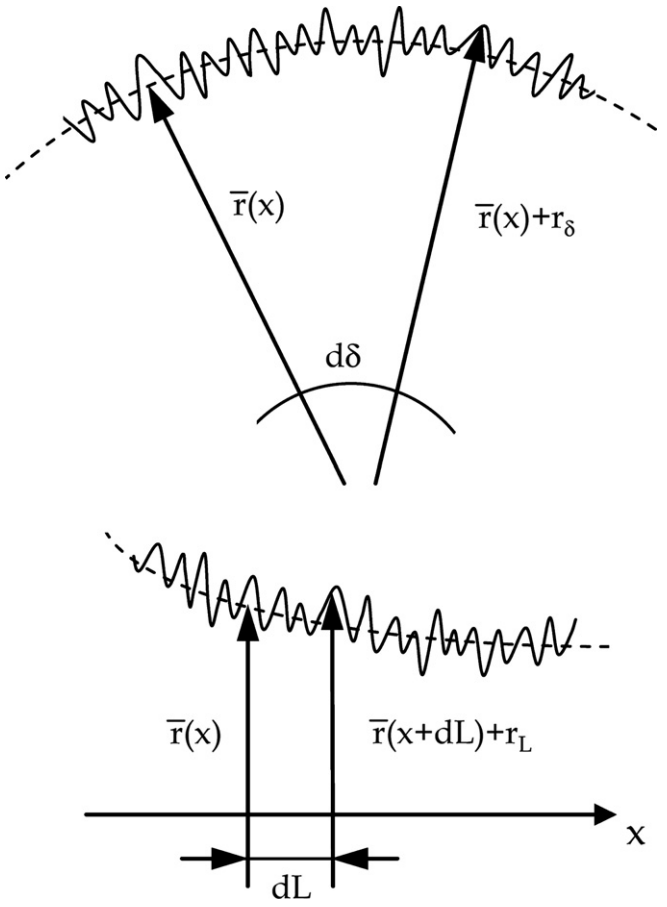

Fig. 2. Details of cross- and longitudinal-sections of a generic pin fin of variable profile and rough surface.

In this way, the model of Ref. [9] essentially consists in taking probabilistic averages of the coefficients of the fin equation, e.g., Eq. (1) above. This "average fin" is subsequently solved and the result compared to the corresponding smooth case to ascertain the effect of roughness. The analytical derivation then amounts to calculate averages for the cross-sectional area A_c, the surface area exposed to convection A_s and their axial variations.

The average cross-sectional area can be calculated from the expression

$$\bar{A}_c(x) = \pi\overline{r(x)^2} = \pi\int_{-\infty}^{\infty}\int_{-\infty}^{\infty}[\bar{r}(x) + r_\delta + r_L]^2\Theta(r_\delta)\Theta(r_L)dr_\delta\, dr_L \tag{26}$$

where the integral limits range from $-\infty$ to ∞, since an unclipped Gaussian distribution has been adopted. Obviously, the probability for such small/large values is quite low. If a change of variables is carried out, $u_\delta = r_\delta/\sigma$ and $u_L = r_L/\sigma$, and the relative roughness ε is specified by using the radius at the fin base,

$$\varepsilon = \frac{\sigma}{r_b} \tag{27}$$

Eq. (26) can be transformed to

$$\overline{A}_c(x) = \frac{1}{2}\int_{-\infty}^{\infty}\int_{-\infty}^{\infty}\left[\frac{\overline{r}(x)}{r_b\varepsilon}+u_\delta + u_L\right]^2 \exp\left(-\frac{u_\delta^2}{2}\right)\exp\left(-\frac{u_L^2}{2}\right)\sigma^2 du_\delta\, du_L \tag{28}$$

Taking into account that the average of u_δ and u_L is nil, and that the average of their squares is, by definition, σ^2, the integral can be easily solved:

$$\overline{A}_c(x) = \pi\overline{r}(x)^2+2\pi r_b^2\varepsilon^2 \tag{29}$$

Now, we may denote by $A_c(x) = \pi\overline{r}(x)^2$ the cross-sectional area of the smooth pin fin whose radius is the same as the average radius of the rough pin fin. Dividing by it, the following factor results as a modifier of the corresponding coefficients in the fin equation:

$$\frac{\overline{A}_c(x)}{A_c(x)} = 1+2\left(\frac{r_b}{\overline{r}(x)}\right)^2\varepsilon^2 \tag{30}$$

We see that the effect of roughness is to increase the circular area by the small amount $\pi\sigma^2$, which, under symmetric, zero mean probability distributions, is obviously an effect of curvature.

To proceed with the remaining coefficients, we need another parameter pertaining to the surface roughness that is not specified by the probability distribution of the radius. It is the mean absolute surface slope of the roughness component, defined as

$$m_\sigma = \frac{1}{L}\int_0^L \left|\frac{\partial(r-\overline{r})}{\partial x}\right| dx \tag{31}$$

The average value of dA_c/dx can be then calculated as

$$\overline{\frac{dA_c}{dx}} = 2\pi\overline{r\frac{\partial r}{\partial x}} = 2\pi\left(\overline{r\frac{d\overline{r}}{dx}}+\overline{r\frac{\partial(r-\overline{r})}{\partial x}}\right) = 2\pi\overline{r}\frac{d\overline{r}}{dx}+2\pi\overline{r\frac{\partial(r-\overline{r})}{\partial x}} \approx \frac{dA_c}{dx}+2\pi\overline{r}(x)m_\sigma \tag{32}$$

In the last step, the average value of the product of the radius times the surface slope is approximated by means of the parameter m_σ. Eq. (32) indicates that a second effect of surface roughness on the average pin fin is to induce an additional axial (x) increase of the cross-sectional area.

Finally, as it is evident, the fin lateral area and apparent perimeter will also increase due to the increase of the length of arc of the profile $d\lambda$. This can be estimated as

$$\overline{dA_s}(x) = 2\pi\overline{r\,d\lambda} \approx 2\pi\overline{r}\sqrt{1+m_\sigma^2}\,dx \tag{33}$$

$$\overline{P}(x) = \overline{\frac{dA_s}{dx}} \approx 2\pi\overline{r}\sqrt{1+m_\sigma^2} \tag{34}$$

so that, for a smooth perimeter $P(x) = 2\pi\overline{r}(x)$, the factor for the equation is

$$\frac{\overline{P}(x)}{P(x)} = \sqrt{1+m_\sigma^2} \tag{35}$$

As in Ref. [9], we note at this point that Eqs. (32)–(35) are only reasonable approximations in terms of the simple parameter m_σ, an essentially empirical piece of information that can be found in the literature addressing surface finishing [14]. Actual correlation between radius and slope in Eq. (32) and total length of arc in Eqs. (33)–(35) are obviously susceptible to dedicated measurement, which would result in precise values, but this is out of the scope of this study.

Concerning the variable-profile pin fins, in Eqs. (33) and (34), we have adopted the usual approximation for a slender fin that $(d\overline{r}/dx)^2 \ll 1$, so that the smooth length of arc is approximately dx. (This is coherent with all the fin equations written above.) It might appear at a first glance that the approximation is valid only when the roughness-induced slope is $m_\sigma^2 \gg (d\overline{r}/dx)^2$, since otherwise the factor must be either

$$\frac{\overline{P}(x)}{P(x)} = \sqrt{1+\left(\frac{d\overline{r}}{dx}\right)^2+m_\sigma^2} \tag{36}$$

or unity. In other words, either the roughness has no effect within the length-of-arc approximation or the approximation cannot be invoked when treating rough fins. The latter possibility is highly undesirable, because the fin equation will then become much more intricate. Fortunately enough, we should remember that m_σ is an average. Even in the common case that $m_\sigma^2 \sim (d\overline{r}/dx)^2$, this expresses only a finite-distance average. Locally at every x, we can expect a much larger effect from roughness than from the average profile slope, as it is graphically illustrated in Fig. 3. Consequently, the length-of-arc approximation is always warranted for the smooth, base profile, and Eqs. (33) and (34) are fully coherent.

Substituting Eqs. (30), (32) and (35) in the fin equations of the class of Eq. (1), we get differential equations describing the temperature change in rough micro-pin fins of truncated hyperbolic, trapezoidal and concave parabolic profiles. They are, in full

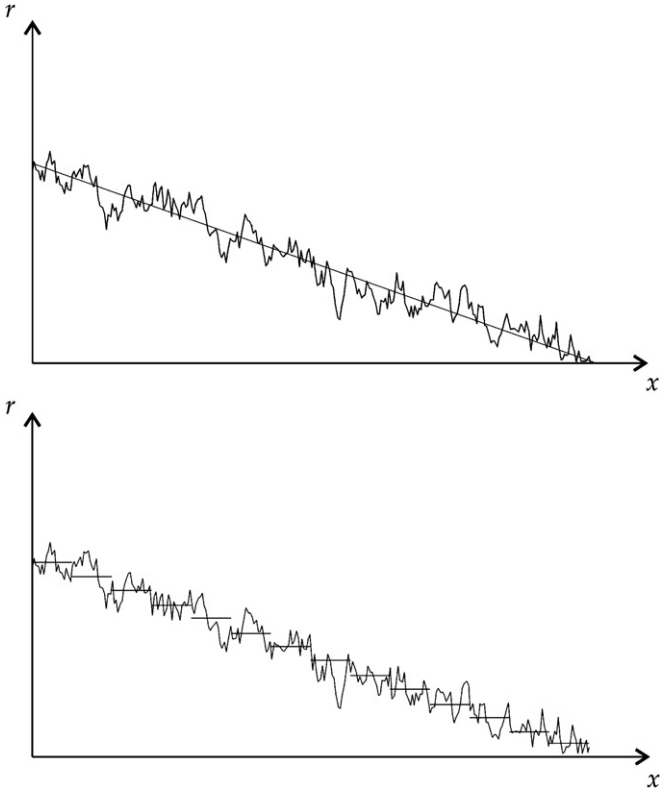

Fig. 3. Length-of-arc idealization in rough micro-fins.

$$\frac{d^2T_h}{dx^2}+2\varepsilon^2\left(\frac{x}{x_b}\right)^2\frac{d^2T_h}{dx^2}-\frac{2}{x}\frac{dT_h}{dx}+\frac{2m_\sigma}{r_b}\frac{x}{x_b}\frac{dT_h}{dx}$$
$$-2\frac{x}{x_b}m^2\sqrt{1+m_\sigma^2}(T_h-T_\infty)=0 \tag{37a}$$

$$\frac{d^2T_t}{dz^2}+2\varepsilon^2\left(\frac{z_b}{z}\right)^2\frac{d^2T_t}{dz^2}+\frac{2}{z}\frac{dT_t}{dz}-\frac{2m_\sigma}{r_b}\frac{z_b}{z}\frac{dT_t}{dz}$$
$$-2\frac{z_b}{z}m^2\sqrt{1+m_\sigma^2}(T_t-T_\infty)=0 \tag{37b}$$

$$\frac{d^2T_p}{dz^2}+2\varepsilon^2\left(\frac{z_b}{z}\right)^4\frac{d^2T_p}{dz^2}+\frac{4}{z}\frac{dT_p}{dz}-\frac{2m_\sigma}{r_b}\left(\frac{z_b}{z}\right)^2\frac{dT_p}{dz}$$
$$-2\left(\frac{z_b}{z}\right)^2m^2\sqrt{1+m_\sigma^2}(T_p-T_\infty)=0 \tag{37c}$$

Invoking the same non-dimensional variables and coefficients as above, we get

$$\psi\frac{d^2\theta_h}{d\psi^2}+2\varepsilon^2\left(\frac{x_t}{x_b}\right)^2\psi^3\frac{d^2\theta_h}{d\psi^2}-2\frac{d\theta_h}{d\psi}+2\frac{x_t^2}{x_br_b}m_\sigma\psi^2\frac{d\theta_h}{d\psi}$$
$$-2M_h^2\psi^2\sqrt{1+m_\sigma^2}\theta_h=0 \tag{38a}$$

$$\phi\frac{d^2\theta_t}{d\phi^2}+2\varepsilon^2\frac{1}{\phi}\frac{d^2\theta_t}{d\phi^2}+2\frac{d\theta_t}{d\phi}-2\frac{z_b}{r_b}m_\sigma\frac{d\theta_t}{d\phi}$$
$$-2M_t^2\sqrt{1+m_\sigma^2}\theta_t=0 \tag{38b}$$

$$\phi\frac{d^2\theta_p}{d\phi^2}+2\varepsilon^2\frac{1}{\phi^3}\frac{d^2\theta_p}{d\phi^2}+4\frac{d\theta_p}{d\phi}-2\frac{z_b}{r_b}m_\sigma\frac{1}{\phi}\frac{d\theta_p}{d\phi}$$
$$-2M_p^2\frac{1}{\phi}\sqrt{1+m_\sigma^2}\theta_p=0 \tag{38c}$$

At this point, it is easy to check that for a smooth pin fin ($\varepsilon\to 0$, $m_\sigma\to 0$) the set of Eq. (37) reduces to the set of Eqs. (6), (12) and (13), and likewise the set of Eq. (38) to that of Eq. (15). We do not purportedly provide exact solutions of these equations, because their forms are much more intricate than the solution for smooth pin fins, Eq. (21). This a side-effect of the roughness model we have applied. Alternatively, the power series method facilitates accurate approximations in an easier way. Before doing that, we rearrange Eq. (38) in order to streamline the nomenclature in forthcoming sections:

$$\psi\frac{d^2\theta_h}{d\psi^2}+2\alpha_h\psi^3\frac{d^2\theta_h}{d\psi^2}-2\frac{d\theta_h}{d\psi}+2\beta_h\psi^2\frac{d\theta_h}{d\psi}-2\chi_h\psi^2\theta_h=0 \tag{39a}$$

$$\phi^2\frac{d^2\theta_t}{d\phi^2}+2\alpha_t\frac{d^2\theta_t}{d\phi^2}+2\phi\frac{d\theta_t}{d\phi}-2\beta_t\phi\frac{d\theta_t}{d\phi}-2\chi_t\phi\theta_t=0 \tag{39b}$$

$$\phi^4\frac{d^2\theta_p}{d\phi^2}+2\alpha_p\frac{d^2\theta_p}{d\phi^2}+4\phi^3\frac{d\theta_p}{d\phi}-2\beta_p\phi^2\frac{d\theta_p}{d\phi}-2\chi_p\phi^2\theta_p=0 \tag{39c}$$

where the participating coefficients α, β and χ are given by

$$\alpha_h=\varepsilon^2\left(\frac{x_t}{x_b}\right)^2,\quad \alpha_t=\alpha_p=\varepsilon^2 \tag{40a}$$

$$\beta_h=\frac{x_t^2}{x_br_b}m_\sigma,\quad \beta_t=\beta_p=\frac{z_b}{r_b}m_\sigma \tag{40b}$$

$$\chi_h=M_h^2\sqrt{1+m_\sigma^2},\quad \chi_t=M_t^2\sqrt{1+m_\sigma^2},\quad \chi_p=M_p^2\sqrt{1+m_\sigma^2} \tag{40c}$$

4. Power series solutions

Analytic solutions of Eq. (39) are sought in terms of the following power series:

$$\theta_h(\psi)=\sum_{i=0}^{\infty}a_i(\psi-1)^i \tag{41a}$$

$$\theta_t(\phi)=\sum_{i=0}^{\infty}a_i(\phi-1)^i \tag{41b}$$

$$\theta_p(\phi)=\sum_{i=0}^{\infty}a_i(\phi-1)^i \tag{41c}$$

where the coefficients a_i ($i=0,1,\ldots,\infty$) are real numbers connected to each pin fin geometry. The domain of the dimensionless temperature θ is generally referred to as the interval of convergence of the power series. The theory specialized on the existence, uniqueness and convergence of power series is available for instance in Ref. [15].

Firstly, we introduce $\theta(\psi)$ or $\theta(\phi)$ from the set of Eq. (41), along with their first and second derivatives, in the set of Eq. (39). For the infinite series to be a solution, the ensuing coefficients of each of the $(\psi-1)$, $(\phi-1)$ terms should be zero. After the algebra is done, the following system of algebraic equations for the coefficients a_i is obtained:

1) For the hyperbolic pin fin,

$$2(1+2\alpha_h)a_2-2(1-\beta_h)a_1-2\chi_ha_0=0 \tag{42a}$$

$$3\cdot 2(1+2\alpha_h)a_3-2[2(1-\beta_h)-(1+6\alpha_h)]a_2$$
$$-(2\chi_h-4\beta_h)a_1-4\chi_ha_0=0 \tag{42b}$$

$$i=2,\ldots,\infty,\quad (i+2)(i+1)(1+2\alpha_h)a_{i+2}$$
$$-(i+1)[2(1-\beta_h)-i(1+6\alpha_h)]a_{i+1}$$
$$-[2\chi_h-4\beta_hi-6\alpha_hi(i-1)]a_i$$
$$-[4\chi_h+(i-1)(-2\beta_h-2\alpha_h(i-2))]a_{i-1}$$
$$-2\chi_ha_{i-2}=0 \tag{42c}$$

2) For the trapezoidal pin fin,

$$2(1+2\alpha_t)a_2+2(1-\beta_t)a_1-2\chi_ta_0=0 \tag{43a}$$

$$i=1,\ldots,\infty,\quad (i+2)(i+1)(1+2\alpha_t)a_{i+2}$$
$$+(i+1)[2i+2(1-\beta_t)]a_{i+1}+[i(i-1)$$
$$+2i(1-\beta_t)-2\chi_t]a_i-2\chi_ta_{i-1}=0 \tag{43b}$$

3) For the concave parabolic pin fin,

$$2(1+2\alpha_p)a_2 + 2(2-\beta_p)a_1 - 2\chi_p a_0 = 0 \quad (44a)$$

$$3\cdot 2(1+2\alpha_p)a_3 + 2\left[4+2(2-\beta_p)\right]a_2 + \left[4(3-\beta_p) - 2\chi_p\right]a_1 - 4\chi_p a_0 = 0 \quad (44b)$$

$$i = 2,\ldots,\infty, \quad (i+2)\,(i+1)\,(1+2\alpha_p)a_{i+2} + (i+1)\left[4\cdot i + 2(2-\beta_p)\right]a_{i+1} + \left[6i(i-1) + 4i(3-\beta_p) - 2\chi_p\right]a_i + \left[4(i-1)\,(i-2) + 2(i-1)\,(6-\beta_p) - 4\chi_p\right]a_{i-1} + \left[(i-2)\,(i-3) + 4(i-2) - 2\chi_p\right]a_{i-2} = 0 \quad (44c)$$

Application of the two boundary conditions for the hyperbolic pin fin as given by Eq. (17) provides

$$a_0 + \sum_{i=1}^{\infty} a_i(\xi-1)^i = 1 \quad (45)$$

$$a_1 = 0 \quad (46)$$

Similarly, application of the two boundary conditions for the trapezoidal and concave parabolic pin fins as given by Eq. (18) leads to

$$a_0 = 1 \quad (47)$$

$$a_1 + \sum_{i=2}^{\infty} i a_i(\omega-1)^{i-1} = 0 \quad (48)$$

For the determination of the heat transfer rates, via the fin efficiencies defined by Eq. (22), the following trio of equations arises

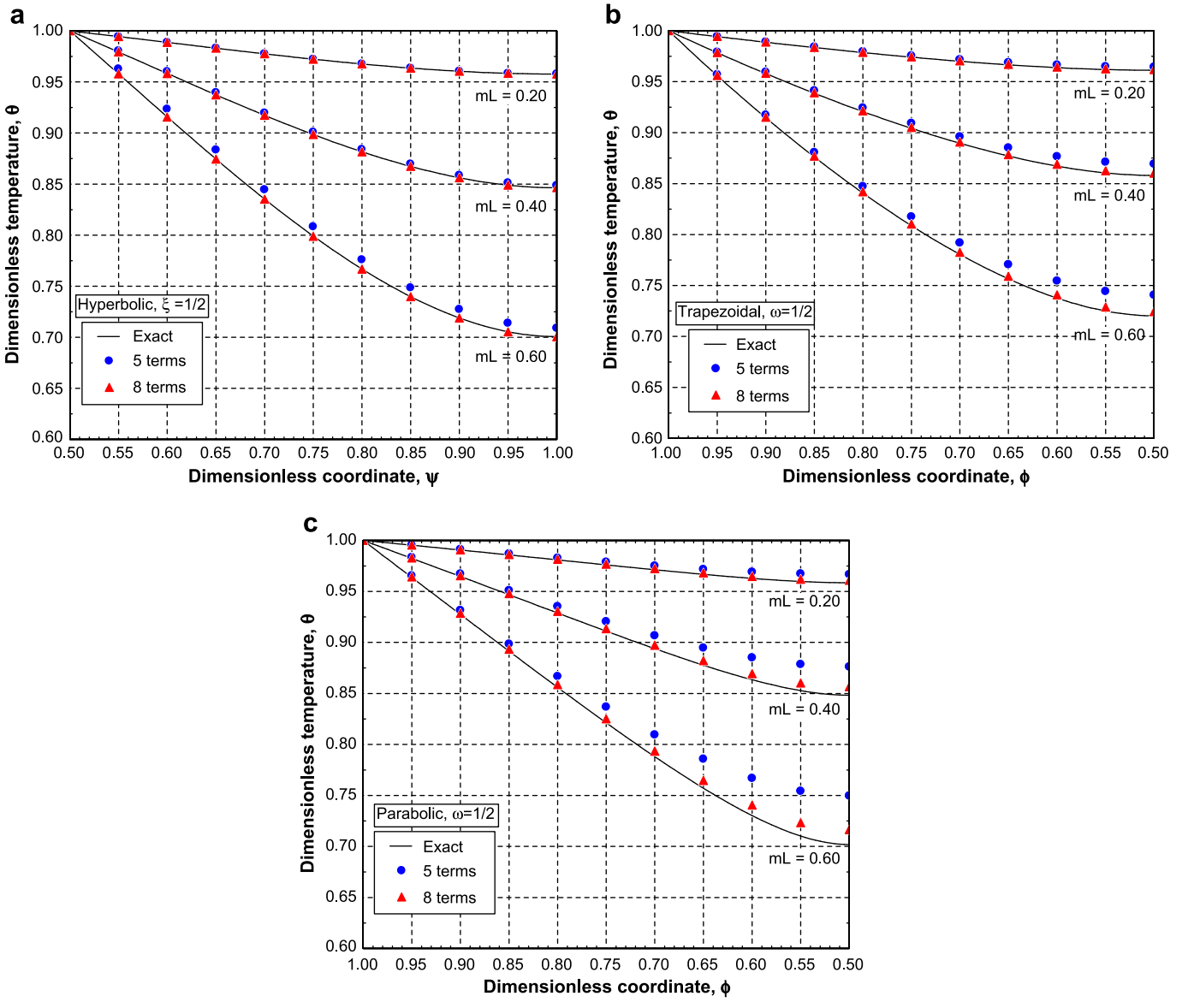

Fig. 4. Dimensionless temperature profile for smooth pin fins ($\varepsilon = 0$): a) hyperbolic, b) trapezoidal, c) concave parabolic.

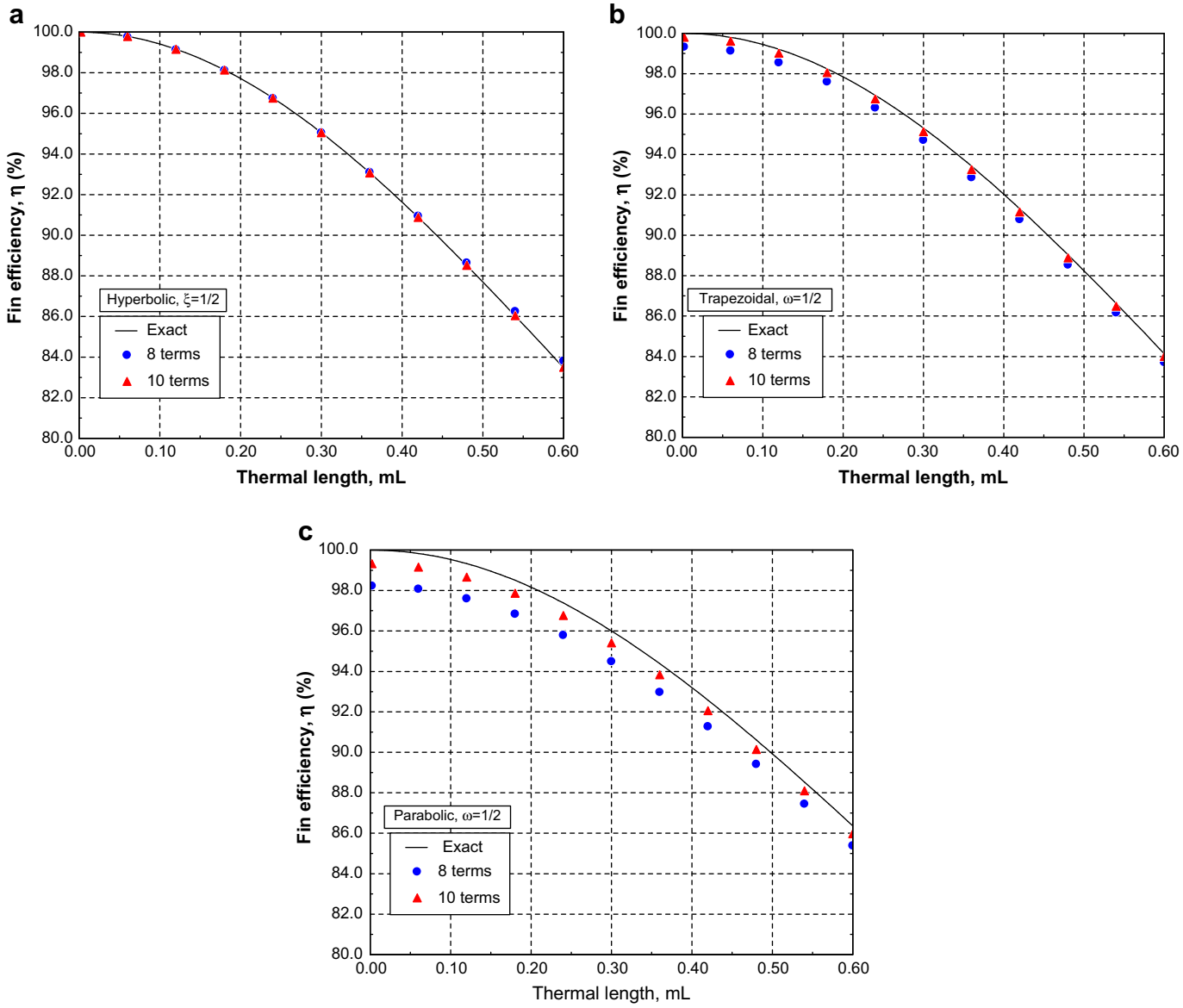

Fig. 5. Fin efficiency versus thermal length for smooth pin fins ($\varepsilon = 0$): a) hyperbolic, b) trapezoidal, c) concave parabolic.

$$\eta_h = -\frac{k}{h}\frac{A_b}{A_s}\frac{1}{x_t}\left[a_1 + \sum_{i=2}^{\infty} i a_i (\xi - 1)^{i-1}\right] \tag{49a}$$

$$\eta_t = -\frac{k}{h}\frac{A_b}{A_s}\frac{1}{z_b} a_1 \tag{49b}$$

$$\eta_p = -\frac{k}{h}\frac{A_b}{A_s}\frac{1}{z_b} a_1 \tag{49c}$$

Table 1
Maximum fractional errors f_θ for the calculation of temperatures of rough micro-pin fins by the power series ($L/r_t = 10$, $Bi = 2 \times 10^{-3}$).

	ε	f_8	f_9	f_{10}	f_{11}	f_{12}
Hyperbolic	0.05	0.0003	0.0003	0.0002	0.0001	0.0001
	0.10	0.0003	0.0002	0.0001	0.0001	0.0001
	0.15	0.0002	0.0002	0.0001	0.0001	0.0001
Trapezoidal	0.05	0.0002	0.0002	0.0002	0.0001	0.0001
	0.10	0.0002	0.0002	0.0002	0.0001	0.0001
	0.15	0.0002	0.0002	0.0001	0.0001	0.0001
Concave parabolic	0.05	0.0001	0.0001	0.0001	0.0001	0.0001
	0.10	0.0001	0.0001	0.0001	0.0001	0.0001
	0.15	0.0001	0.0001	0.0001	0.0001	0.0000

Finally, for the computation of the fin effectivenesses defined by Eq. (23), the trio of equations turns out to be

$$E_h = -\frac{k}{h}\frac{1}{x_t}\left[a_1 + \sum_{i=2}^{\infty} i a_i (\xi - 1)^{i-1}\right] \tag{50a}$$

$$E_t = -\frac{k}{h}\frac{1}{z_b} a_1 \tag{50b}$$

$$E_p = -\frac{k}{h}\frac{1}{z_b} a_1 \tag{50c}$$

The cross-sectional area at the base and the lateral surface area of the rough pin fins have been averaged for the calculation of the efficiencies and effectivenesses, incorporating the modifier factors $1+2\varepsilon^2$ and $\sqrt{1+m_\sigma^2}$ arising in Eqs. (30) and (35) respectively.

Conceptually, a convergent infinite series is by definition identical to the exact solution. If instead a finite number of terms n is retained, an approximate solution is obtained, which can be accurate and easier to evaluate. The key step is to test the convergence of the series by comparing the approximate solutions obtained from the shortened series $\theta_n(\psi)$ or $\theta_n(\varphi)$ against the exact solution $\theta(\psi)$ or $\theta(\varphi)$. Since the latter is not undertaken for the rough fin, we proceed for the smooth micro-pin fins i.e., for the particular situation with $\varepsilon=0$ and $m_\sigma=0$ as given by Eq. (21). Once an appropriate number of terms n is selected, we extend the truncated series to incorporate the effect of the surface roughness. In absence of the exact solution, a criterion of relative convergence is applied to assure the accuracy of the solution.

5. Presentation of results

The exact temperature distributions come from the evaluation of the set of Eq. (21), the exact fin efficiencies from the set of Eq. (22) and the exact fin effectivenesses from the set of Eq. (23). They have been conveniently computed with the software Mathematica [12]. The approximate temperature distributions $\theta_n(\psi)$ or $\theta_n(\phi)$ and the approximate fin efficiencies and effectivenesses η_n and E_n have been calculated by means of a short computer program written for that purpose.

The three-part Fig. 4 displays dimensionless temperature θ on the ordinate and dimensionless coordinate ψ or ϕ on the abscissa for a given geometric ratio ξ or ω. As the third, independent parameter, we use the dimensionless fin parameter mL (sometimes called the fin "thermal length"). It is a matter of algebra to deduce the relationship with the original variable, viz., the extended Biot number M_h, M_t, M_p in Eq. (21):

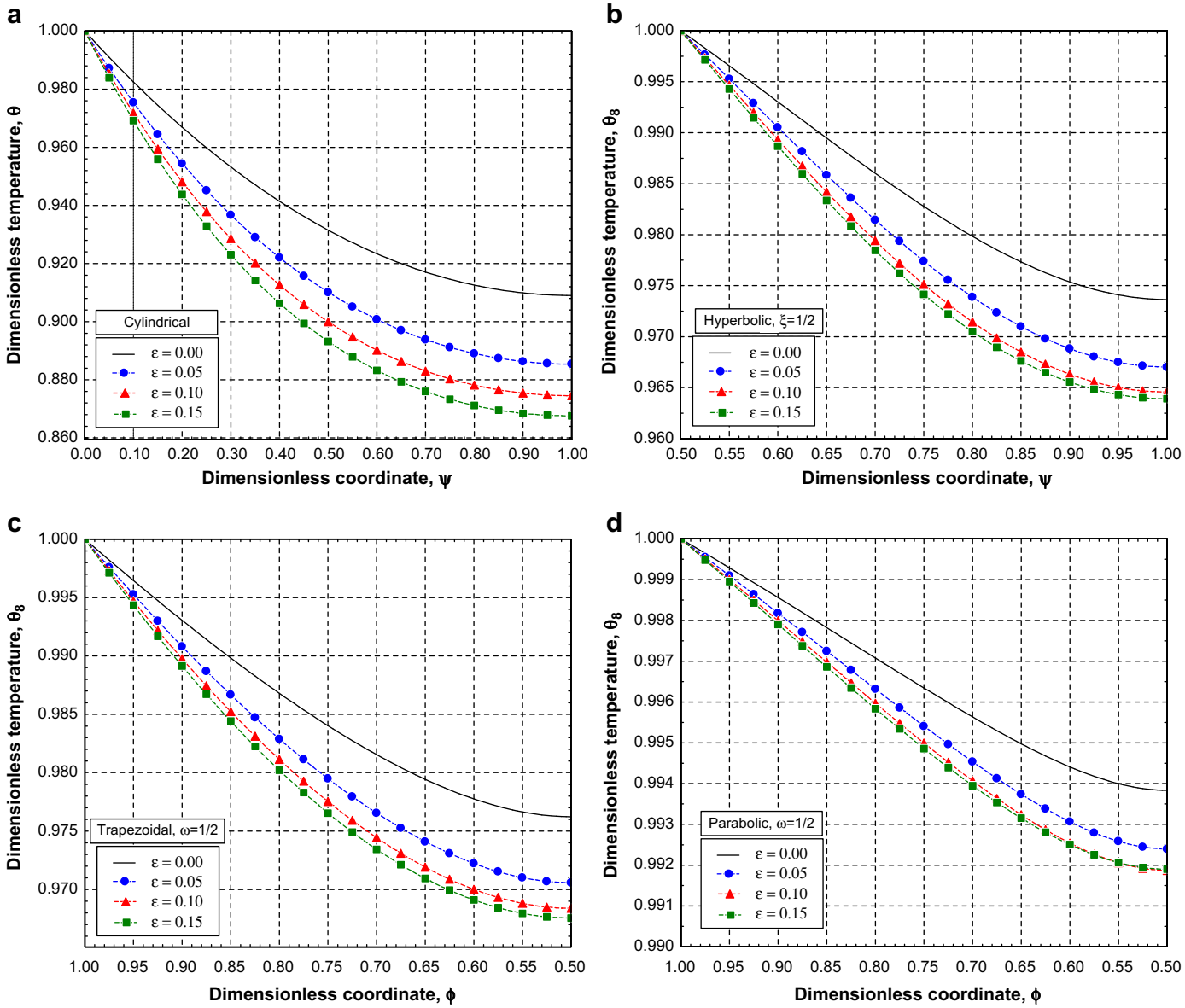

Fig. 6. Effect of surface roughness on temperature profile of micro-pin fins ($L/r_t=10$, $Bi=2\times10^{-3}$): a) cylindrical, b) hyperbolic, c) trapezoidal, d) concave parabolic.

$$mL = \sqrt{\xi}(1-\xi)M_h = \frac{L}{r_t}\xi\sqrt{\frac{Bi}{2}} \quad (51a)$$

$$mL = (1-\omega)M_t = \frac{L}{r_t}\omega\sqrt{\frac{Bi}{2}} \quad (51b)$$

$$mL = (1-\omega)M_p = \frac{L}{r_t}\omega^2\sqrt{\frac{Bi}{2}} \quad (51c)$$

We use mL since this is very common in fin theory and also because its value is less than unity for normal applications. For future reference, we also include in Eq. (51) the Biot number Bi; in this way, mL is related with the pairs (M_h, ξ), (M_t, ω), (M_p, ω) or the pairs (Bi, ξ), (Bi, ω) for $L/r_t = \text{const}$.

The results plotted in Fig. 4, provided for arbitrary geometric ratios $\xi = ½$ and $\omega = ½$, indicate that temperature distributions are predicted very accurately by the approximate 8-term series θ_8. Maximum discrepancies arise in the tip temperature for the largest mL; they amount to 0.02%, 0.56% and 2.09% of the exact values, for the hyperbolic, trapezoidal and concave parabolic pin fins, respectively. Even the approximate temperature predictions with a shorter 5-term series θ_5 are fairly good; this is especially true for low mL values (as will be the case in practical applications).

In Fig. 5, the fin efficiencies η of the basic smooth pin fins are represented versus mL for the same geometric ratios $\xi = ½$ and $\omega = ½$. Calculations with the shortened 10-term series η_{10} lead to an accurate prediction, the maximum differences being between 0.03% and 0.67% of the exact values. As in Fig. 4, the error is the largest for the concave parabolic pin fin, which suggests a direct influence of volume optimality.

It should be emphasized that the predictions shown in Figs. 4 and 5, given in terms of dimensionless groups, are valid for any broad heat transfer application and not only for specific arrangements used in micro-devices. Conversely, these figures also serve to initially test the number of terms that could be expected for rough micro-pin fin simulations. To this purpose, the following ratios are used to test the convergence of the series within a fractional error:

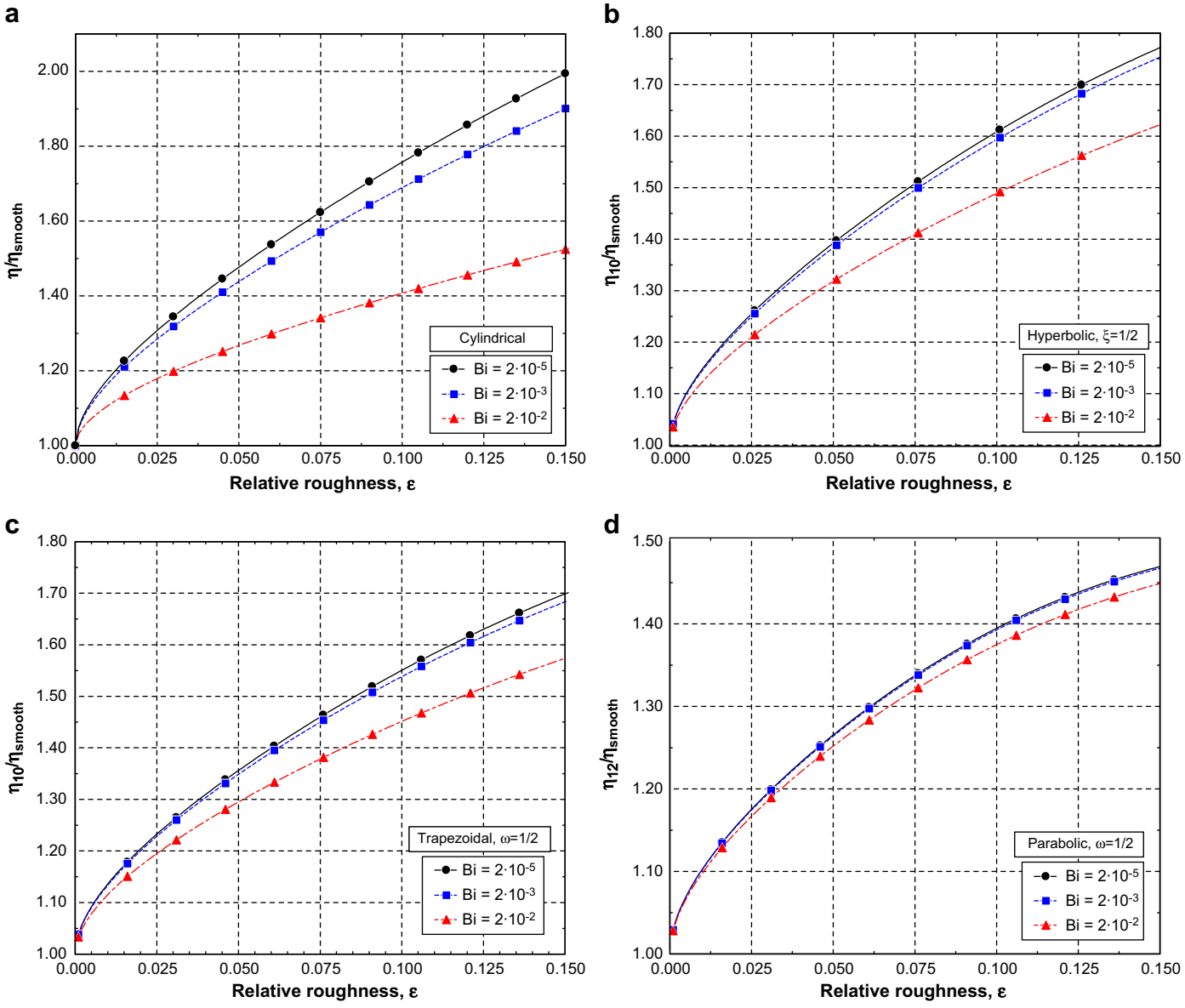

Fig. 7. Effect of surface roughness on efficiency of micro-pin fins ($L/r_t = 10$): a) cylindrical, b) hyperbolic, c) trapezoidal, d) concave parabolic.

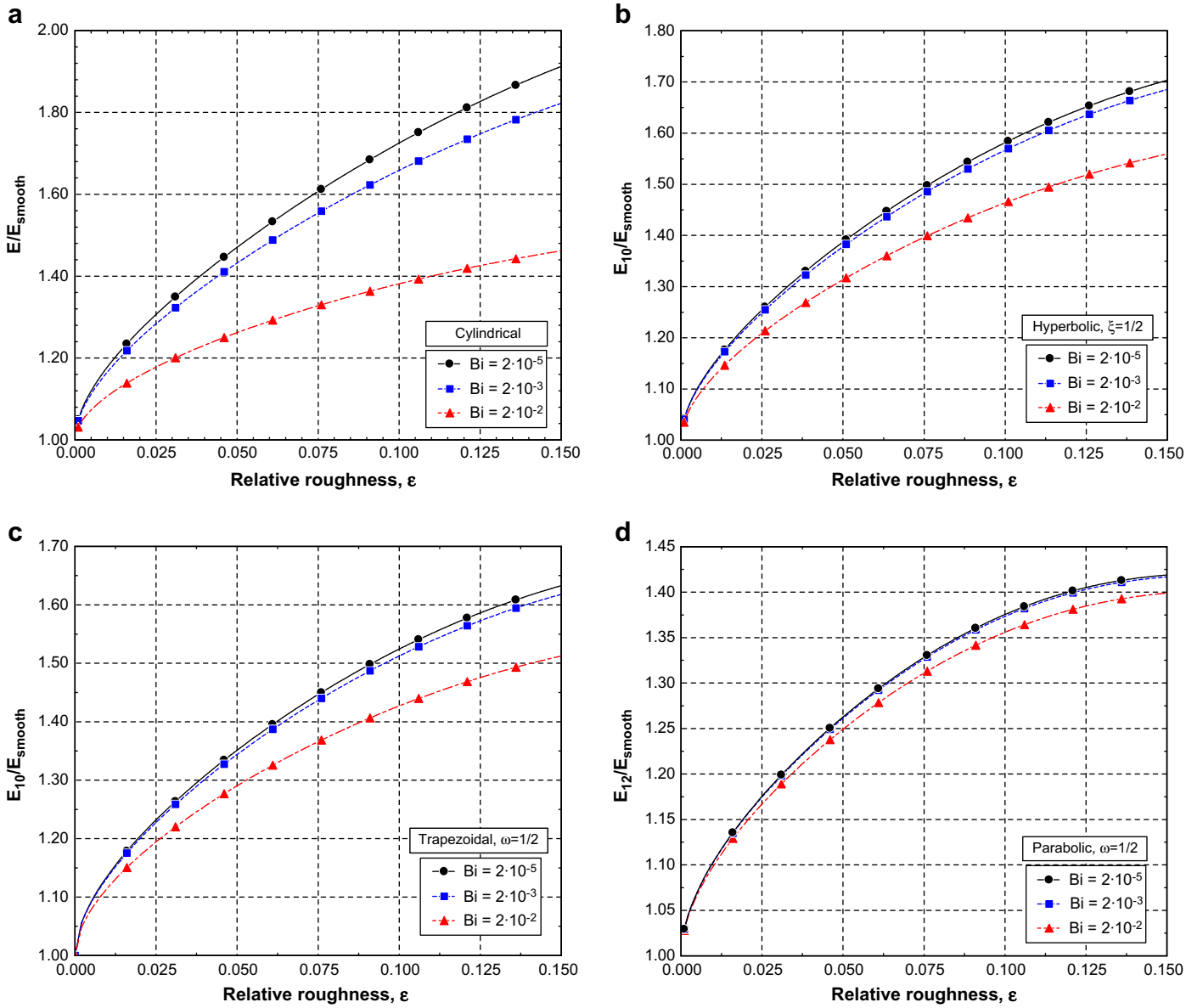

Fig. 8. Effect of surface roughness on effectiveness of micro-pin fins ($L/r_t = 10$): a) cylindrical, b) hyperbolic, c) trapezoidal, d) concave parabolic.

$$f_\theta = \left|\frac{\theta_n - \theta_{n-1}}{\theta_n}\right| < e \tag{52a}$$

$$f_\eta = \left|\frac{\eta_n - \eta_{n-1}}{\eta_n}\right| < e \tag{52b}$$

$$f_E = \left|\frac{E_n - E_{n-1}}{E_n}\right| < e \tag{52c}$$

Table 1 summarizes the errors associated with the approximate temperature computations of rough micro-pin fins when the number of terms is progressively increased. These results have been obtained for a representative example: typical values for micro-pin fins dimensions ($r_t = 5$ μm, $L = 50$ μm), Biot number $Bi = 2 \times 10^{-3}$, and three values of the relative roughness $\varepsilon = 0.05$, 0.10, 0.15, as suggested in Ref. [9]. As stated above, validity of the rough fin model is only warranted for a relative roughness $\varepsilon \ll 1$, but we retain a range 0–0.15 for comparison purposes. In most applications, ε will typically be lower than 0.05. In addition, to proceed with the calculations, we have selected the following empirical expression for the mean absolute slope of the surface roughness [14]

$$m_\sigma = 0.076\sigma^{0.52} \tag{53}$$

where σ is in micrometers. It is clear from Table 1 that increasing the number of terms beyond ≈8 does not yield any significant improvement of accuracy. For this reason, we have taken the predictions given by θ_8 to simulate the temperature patterns in the micro-pin fins in an adequate manner, even though a smaller number of terms would have likely produced acceptable results. The same procedure has been applied to the prediction of efficiency and effectiveness of the rough pin fins: to assure a convergence error lower than 0.5% for all computed cases, 10-term series are required for the hyperbolic and trapezoidal simulations and 12-term series for the case of the concave parabolic pin fin.

Fig. 6 pictures the effect of surface roughness on the temperature distribution along the fin length, as calculated by the power series. We have also included, for comparison purposes, results for the constant-diameter case; its exact analytical solution can be consulted in Ref. [9]. The results obtained for variable diameter follow the same trend; differences in absolute values for the temperature descent come both from the different profile geometry and from the different fin base radius r_b (for which the Biot number is defined).

Temperature trends are confirmed by the calculation of fin-quality ratios. Fig. 7 displays the effect of the relative roughness ε on the efficiency η, taking as a reference the efficiency for the smooth geometry. Three different values of Biot number $Bi = 2 \times 10^{-5}$, 2×10^{-3}, 2×10^{-2} have been included, preserving a difference of three orders of magnitude. Even for values of $\varepsilon \leq 0.05$, the effect on fin efficiency can be substantial: an increase up to 25–40%, which is fully coherent with the original calculations of Ref. [9]. Fig. 8 displays the effect on the effectiveness ratio E_{rough}/E_{smooth}, showing a similar trend. In all the graphs, we see that the benefit gained with roughness is the largest for hyperbolic pin fins and the smallest for concave parabolic, and so is the parametric effect of Bi and ε; this is again related to volume optimality.

As for the reasons of this significant improvement of fin performance, some insight can be gained by comparing Eq. (15) for smooth fins with Eq. (38) that incorporate the modeled effect of roughness. For the example of a hyperbolic fin with $\xi = 0.5$ and a value of roughness $\varepsilon = 0.05$, the coefficients of the three terms of the equation increase for the rough case with reference to the smooth one in the following relative magnitudes:

- Term in $d^2\theta_h/d\xi^2$: 0.5–2%.
- Term in $d\theta_h/d\xi$: 13–106%.
- Term in θ_h: 0.14%.

The ensuing analysis is thus rather clear. According to the statistical model of rough fins, the increase in efficiency (30–40% in this case) is mostly due to the first derivative term, i.e., to the correlation of radius and roughness slope. A much minor contribution can be attributed to the increase of cross-sectional area (second derivative). The increase of perimeter (independent term) is negligible.

Even considering the fact that a change of coefficients of a differential equation, even a linear one, cannot be directly related to the change in its solution, this is of course interesting and perhaps deserves more investigation. In this respect, the original application of the model [9] deals with a constant-diameter fin, and thus always changes the first derivative term in an infinite relative amount, since this is indeed absent for the smooth geometry.

6. Conclusions

The influence of a random, isotropic surface roughness on truncated micro-pin fins of variable diameter has been investigated for the hyperbolic, trapezoidal and concave parabolic geometries. Theory for the geometric effect of surface roughness presented in Ref. [9] has been generalized to this purpose. Since resulting equations are very complex, an approximate method has been adopted. Results are in accordance with those found for constant diameter [9], exhibiting significant improvements in thermal performance.

The approximate method is based on truncated power series. Approximate 5- to 8-term series are accurate for the prediction of temperature distributions, and 8- to 12-term series serve to accurately estimate the efficiency and effectiveness in the case of smooth pin fins. Relative convergence studies show that these figures are practically the same for rough micro-pin fins. The method is easily manageable, offering considerable economy without sacrificing reliability. It can also facilitate the treatment of other smooth or rough micro-geometries of pin, straight and annular fins.

References

[1] A.D. Kraus, A. Aziz, J.R. Welty, Extended Surface Heat Transfer, John Wiley, New York, 2000.
[2] R.L. Webb, Principles of Enhanced Heat Transfer, John Wiley, New York, 1994.
[3] A.D. Kraus, A. Bar-Cohen, Design and Analysis of Heat Sinks, John Wiley, New York, 1997.
[4] C. Marques, K.W. Kelly, Fabrication and performance of a pin fin micro heat exchanger, Journal of Heat Transfer 126 (2004) 434–444.
[5] Q. Huang, N.K.S. Lee, Analysis and design of polysilicon thermal flexture actuator, Journal of Micromechanics and Microengineering 9 (1999) 64–70.
[6] R. Maboudian, Surface processes in MEMS technologies, Surface Science Reports 30 (1998) 207–269.
[7] E. Achenbach, The effect of surface roughness on the heat transfer from a circular cylinder to the cross flow of air, International Journal of Heat and Mass Transfer 20 (1977) 359–369.
[8] H. Honda, J.J. Wei, Enhanced boiling of FC-72 on silicon chips with micro-pin-fins and submicron-scale roughness, Journal of Heat Transfer 124 (2002) 383–390.
[9] M. Bahrami, M.M. Yovanovich, J.R. Culham, Role of random roughness on thermal performance of microfins, Journal of Thermophysics and Heat Transfer 21 (2007) 153–157.
[10] M.K. Chyu, Y.C. Hsing, V. Natarajan, Convective heat transfer of cubic fin arrays in a narrow channel, Journal of Heat Transfer 120 (1998) 362–367.
[11] A. Mills, Basic Heat Transfer, second ed. Prentice-Hall, Upper Saddle River, New Jersey, 1999.
[12] Wolfram Research Inc., Mathematica 5.2 for Microsoft Windows. www.wolfram.com (2005).
[13] M. Abramowitz, A. Stegun, Handbook of Mathematical Functions with Formulas, Graphs and Mathematical Tables, Ninth Printing, Dover, New York, 1972.
[14] M.A. Lambert, L.S. Fletcher, Thermal contact conductance of spherical rough metals, Journal of Heat Transfer 119 (1997) 684–690.
[15] E.L. Ince, Ordinary Differential Equations, Dover, New York, 1956.